

Incremental-Compensation Based Low-Cost Offline Robust Topology Control for Micro/Nano Satellite Network

ZHAO LI^{1,2}, YUYU HU¹, ZHENDONG HU¹, JINGLING LI³,
SHITONG ZHU¹ AND YANG XU¹

¹*School of Cyber Engineering, Xidian University
Xi'an, Shaanxi, 710126 P.R. China
E-mail: zli@xidian.edu.cn*

²*Science and Technology on Communication Networks Lab.
54th Research Institute of China Electronics Technology Group Cooperation
Shijiazhuang, Hebei, 050081 P.R. China*

³*National Key Lab. of Science and Technology on Space Microwave
China Academy of Space Technology
Xi'an, Shaanxi, 710199 P.R. China*

With the rapid development of micro-electronic technologies, micro/nano satellites are becoming more attractive. Micro/Nano satellites have the advantages of fast deployment, low cost and flexible application. By building them into a network, their advantages in performing various types of space tasks can be further exploited. Since maintaining connectivity is critical to the use of micro/nano satellite network and satellite nodes are subject to limited onboard resources, design of low-cost robust topology control is of great research significance. Although k -connectivity topology control can achieve good robustness, they may yield large link redundancy and control overhead. Therefore, in this paper, we will propose an incremental-compensation based robust topology control (ICRTC) algorithm to balance the redundant link overhead and network's robustness. By establishing backup link(s) with respect to the fragile link(s) associated with the high-failure-probability nodes, ICRTC can enhance network's robustness with proper link redundancy cost. Moreover, by taking practical limitations of micro/nano satellites into consideration, we present a low-cost offline realization of ICRTC. Under this implementation, the orbit period is first divided into a series of time slots, and for each slot a topology snapshot is computed, so that a snapshot sequence is obtained. Next, we preprocess the above sequence by combining successive snapshots of the same topology in it so as to reduce its redundancy. Then, ICRTC is applied to each preprocessed snapshot, yielding a compensated snapshot sequence. At last, we merge similar snapshots in the compensated sequence by adding some redundant links to further decrease sequence redundancy. Our simulation results have verified the effectiveness of and shown the benefits brought by ICRTC. Moreover, it has been shown that the topology control overhead can be effectively reduced with the proposed offline realization.

Keywords: micro/nano satellite network, topology control, compensation, robustness, offline

1. INTRODUCTION

With the rapid development of micro-electronic techniques, electronic devices' weight and size are becoming lighter and smaller, promoting the research and applica-

Received December 17, 2020; revised January 30, 2021; accepted March 7, 2021.
Communicated by Changqiao Xu.

tion of micro/nano satellite (1kg–100kg) [1]. Compared to traditional large satellite, micro/nano satellite is smaller, lighter, less expensive, and can be deployed in a more flexible way [2]. Owing to the use of more advanced micro-electronic and micro-mechanic technologies, micro/nano satellites can be networked to perform complex space tasks. As the research goes deeper, micro/nano satellites are expected to be applied to both military and commercial fields. For example, in Earth observation, micro/nano satellites can be launched in batch and networked/formed into a constellation, expanding the observation area and shortening the revisit time [3]. Moreover, since micro/nano satellites are difficult to be detected and attacked, they are promising to be used in military and anti-terrorist communication.

In order to fully exploit the advantages of micro/nano satellites, networking a group of satellites becomes attractive. In micro/nano satellite network, multiple satellites can collaborate with each other via inter-satellite links to complete complex space missions [4,5]. Therefore, ensuring connectivity of micro/nano satellite network is critical to realizing its function properly. Topology control is an important way to maintain network connectivity [6]. This topic has been under extensive study for a long time, outputting numerous algorithms for managing various types of networks' topology. Based on the degree of connection, these algorithms can be classified into single-connected methods, *e.g.*, the unit disk graph (UDG) [7], the minimum spanning tree (MST) [8] and the relative neighbor graph (RNG) [9], and k -connected algorithms, such as cone-based topology control (CBTC) [10] and fault-tolerant global spanning subgraph/fault-tolerant local spanning subgraph (FGSS/FLSS) [11]. With single-connected methods, at most one communication path (a path may consist of multiple one-hop links) is established between a node-pair. This type of methods is featured as low-cost and easy deployment. However, they are subject to network faults incurred by node failure or/and link disconnection. As a comparison, k -connected methods allow multiple paths to be set up between one node-pair, hence yielding better fault-tolerance performance. However, higher complexity is incurred from maintaining multiple paths and redundant links; this may be unacceptable for energy-constraint networks.

Although topology control strategy is regarded as one of the key technologies in satellite networks, it has seldom been studied in recent years, as stated in [12]. The authors of [12] focused on the problem of topology control in satellite cluster networks (SCNs) performing some emergency Earth observation missions, and proposed a topology control strategy to assure reliability where the relative motion, unstable and periodic changes in network topology were considered, so that inter-satellite links (ISLs) can carry out stable data transmission. In [13], a complex space information network was first decoupled into a series of autonomous system (AS) networks; then a topology control algorithm preserving the k -connectivity of the original network was proposed so as to minimize the time delay among the AS networks. In [14], a hybrid topology for distributed satellite clusters involving two types of satellite nodes, *i.e.*, traffic satellite and switch satellite, was proposed so as to realize high reliability, flexibility, and low implementation complexity.

Some research works focus on the dynamic feature of satellite networks in the design of topology control strategies [15-21]. [15] systematically quantified the dynamical activities of regular low earth orbit (LEO) satellite network topologies. The number and length of network snapshots were formulated concisely. With this work, it compensated for the simplified topological assumptions in many LEO satellite network related researches. In

[16], network topology and routing in LEO satellite networks were discussed with consideration of the dynamic nature of satellite networks, based on which a software defined network (SDN) enabled LEO constellation satellite network driven by means of SDN was proposed to realize the integration of satellite and terrestrial networks. By noting that the high density of new constellations and high-velocity nature of such systems render traditional approaches for network design ineffective, the authors of [17] proposed one method explicitly aiming at tackling the high temporal dynamism inherent to low-Earth orbit satellites by exploiting repetitive patterns in the network topology to avoid expensive link changes over time, while still providing near-minimal latencies at nearly $2\times$ the throughput of standard past methods. In [18], topology-adapting routing strategy for the global navigation satellite system (GNSS) was studied. Specifically, the authors first proposed a design method of the ISL scheme based on fixed topology; and then, they formulated a multi-objective optimization and multi-constraint routing model. The authors of [19] addressed the topological dynamics of LEO satellites, and proposed a topological dynamics shielding method named as celestial sphere division based virtual node (CSD-VN) for LEO satellite networks by establishing a static virtual network in space. The authors of [20] presented an ISL reassignment method to optimize the snapshot routing performance for the polar-orbit LEO satellite networks. With this method, when the snapshot routing tables are switching in all satellites, the inter-plane ISLs are regularly reassigned to improve the quality of the next snapshot. The authors of [21] employed the space-time topology graph to describe the connectivity of satellites at different time points as time progresses. The time is equally divided into small slots with the same size. They proposed a collaborative scheme that allows satellites to offload data among themselves using ISLs before they come to the contact with the Earth station (ES), so that satellites will carry the right amount of data according to the length of their contact time with the ES and the throughput of data downloading at ES is maximized.

There are also topology control research works in other types of networks based on which satellite network topology control algorithms can be developed. For example, the authors of [22] proposed logical k -connected topology control algorithms, including both the purely centralized and the purely distributed, based on a hierarchical integrated network including not only SCNs, but also the unmanned aerial vehicles (UAVs) and wireless sensor networks (WSNs). [23] studied the topology control problem in a predictable delay tolerant network (DTN) where the time-evolving network topology is known a priori or can be predicted, and modeled such time-evolving network as a directed space-time graph including both spacial and temporal information. Via topology control, a sparse structure from the original space-time graph can be built. Then, two greedy-based methods were proposed to reduce the total cost of topology while maintaining the connectivity over time.

However, methods applied to LEO satellite networks and other types of ground networks may not be suitable for micro-nano satellite network. By noting that micro/nano satellite carries limited fuel, the space environment is always tough, and the unreliability of hardware and software on the satellite may cause node failure, designing robust topology control algorithms to counteract the abovementioned threats is significant for the application of micro/nano satellite network. It is obvious that the single-connected topology is not fault-tolerant, hence is too fragile to be suitable for micro/nano satellite network. On the other hand, although k -connected topology control can improve network

robustness, it may incur large link redundancy and administrative overheads. Therefore, how to balance the redundancy and the robustness of the network via proper topology control is of research significance.

Moreover, as for the implementation of topology control for micro/nano satellite network, there are two candidate ways, *i.e.*, online real-time control and offline non-real-time control [1, 24], for selection. With online topology control, the satellite network topology is generated and adjusted dynamically so that the influence of satellite node or link failure to the network can be adapt to in time, and hence good network performance can be guaranteed [25]. However, more onboard computational resource, bandwidth and transmit power may be consumed for signaling exchange, topology computation and network management. As for the offline topology control methods, they pre-calculate the snapshots of network topology at different time instants, and then upload this information to satellite nodes to realize network topology control. This type of methods can reduce onboard resource consumption and control overhead, however, precise real-time control is sacrificed [26]. In the design of offline topology control, the shorter the time interval of two successive snapshots, the more precise the snapshot sequence can represent the network. However, in such a case, more onboard storage resource is required, and the network is frequently checked to determine whether its topology need adjustment or not; this may yield frequent topology adjustment and hamper the continuity of data transmission. Noting that micro/nano satellites move along pre-defined orbit, connections between the satellite nodes vary periodically along with time. Therefore, by exploiting periodicity of satellite network, topology control can be realized with reduced redundancy of snapshot sequence while making the network adapt to its working environment.

Based on the above observations, we propose a low-cost offline incremental-compensation based robust topology control (ICRTC) method for micro/nano satellite network. With ICRTC, a single-connected topology is first generated, then the nodes with high failure probability are selected for compensation. The compensation is realized by establishing backup link(s) with respect to (w.r.t.) the fragile link(s) associated with high-failure-probability nodes. In such a way, the network can work properly in the case of node failure while the link redundancy can be well controlled. Then, for the realization of ICRTC, we propose a low-cost offline implementation by exploiting the periodicity feature of satellite network. By combining the successive snapshots having the same topology and merging similar snapshots via adding a few redundant links, so that onboard storage consumption and the network's adaptivity to environment can be balanced.

The main contributions of this paper are two-fold:

- Proposal of incremental-compensation based robust topology control (ICRTC) method. With ICRTC, we select the nodes with high failure probability and add compensation link(s) to these nodes so as to enhance network's robustness with a reasonable link redundancy.
- Proposal of a low-cost offline realization of ICRTC. We first divide the orbit period in multiple time slots, for each of the slots a topology snapshot is computed. Then, we examine all of the snapshots successively and combine the same ones to decrease the redundancy. After that, we merge adjacent similar snapshots by employing some redundant links to further reduce redundancy and the number of

snapshots uploaded to the satellite nodes. In this way, the topology control overhead such as onboard storage burden can be effectively alleviated.

The rest of this paper is organized as follows. Section 2 describes the system model, while Section 3 designs ICRTC. Section 4 analyzes the end-to-end transmission reliable probability, and Section 5 presents a low-cost offline implementation of ICRTC. Section 6 evaluates the performance of proposed method. Finally, Section 7 concludes the paper.

2. SYSTEM MODEL

The orbit of a micro/nano satellite network can be represented in terms of its coordinate system. In this paper, we employ Earth centered inertial (ECI) [27] as shown in Fig. 1. As the figure shows, the origin is at the center of the Earth, and the equatorial plane is chosen as the reference plane. X-axis points to the mean equinox, while Y-axis is obtained by rotating X-axis 90 degrees to east in the equatorial plane. Z-axis is orthogonal to the equatorial plane pointing to North Pole. The above coordinate system employs Kepler orbital elements, including semi-major axis a , eccentricity e , orbit inclination θ , right ascension of the ascending node Ω , argument of perigee ω , and mean anomaly M , to present the orbiting of a group of networked satellites. Note that a equals to the sum of Earth radius and orbit altitude. Then, we can have the expression of Kepler orbital elements as:

$$\mathbf{K} = [a \ e \ \theta \ \Omega \ \omega \ M]. \quad (1)$$

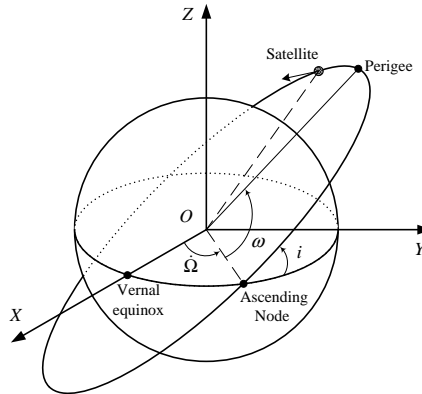


Fig. 1. ECI coordinate system.

As for the micro/nano satellite network, we consider N nodes involved in the network. Then, the network can be modeled as a graph $G = (\Omega_V, \Omega_E)$ where $\Omega_V = \{V_1, \dots, V_n, \dots, V_N\}$ and $\Omega_E = \{E_{(V_i, V_j)}\}$ ($V_i, V_j \in \Omega_V$) are the vertex (satellite) set and edge/link (undirected inter-satellite link) set, respectively. The value/weight of an edge $E_{(V_i, V_j)}$ is determined by the physical distance between nodes V_i and V_j . All the satellites are located in the ECI coordinate system [27]. They move in a circular orbit, *i.e.*, the influence of perturbation forces from other celestial bodies other than the Earth is ignored. We

Table 1. Major parameters.

Symbol	Definition
G	The graph used for representing a micro/nano satellite network
Ω_V	Vertex (satellite) set of graph G
V_i	Satellite node indexed by i
Ω_E	Edge/link (undirected inter-satellite link) set of graph G
$E_{(V_i, V_j)}$	Edge/link connecting node V_i and V_j
A	The cardinality, <i>i.e.</i> , the number of elements, of set A
G_{Init}	The graph used for representing the initial topology of a network obtained by applying MST
$\Omega_{V, Init}$	Initial vertex (satellite) set of graph G_{Init}
$\Omega_{E, Init}^{MST}$	Initial edge/link set of graph G_{Init}
G_{Tgt}	The graph used for representing the target topology obtained by applying ICRTC
$\Omega_{V, Tgt}$	Target vertex (satellite) set of graph G_{Tgt}
$\Omega_{E, Tgt}$	Target edge/link set of graph G_{Tgt}
τ	The number of compensation times
$\Omega_{E, \tau}$	The edge/link set after the τ th compensation
P_V	Node-failure probability set
p_{V_n}	Failure probability of node V_n
$p_{E_{(V_i, V_j)}}$	Failure probability of link $E_{(V_i, V_j)}$
$\hat{\Omega}_V$	The set of nodes for compensation
\hat{V}_n	The node indexed by n in $\hat{\Omega}_V$ for compensation
ρ	The maximum number of compensation times
η	The target end-to-end transmission reliable probability
Ω_V^*	The set of nodes with only one degree
V_m^*	The node indexed by m in Ω_V^*
K	The number of end-to-end node-pairs
Ψ	The number of possible paths between a node-pair
ξ_l	The link set constituting the l th path of a node-pair (excluding the links associated with the end nodes of the path)
$\Phi_{\{V_i^*, V_j^*\}, \tau}$	The end-to-end transmission reliable probability of node-pair $\{V_i^*, V_j^*\}$ via a path denoted by $\{V_i^*, \xi_l, V_j^*\}$ after the τ th compensation
$\Phi_{\{V_i^*, V_j^*\}, \tau}^{[\Psi]}$	The end-to-end transmission reliable probability of node-pair $\{V_i^*, V_j^*\}$ via Ψ possible paths after the τ th compensation
\mathbf{A}	Adjacency matrix of a topology snapshot
\mathbf{Q}_ε	Difference matrix of adjacent matrices in two successive topology snapshots
S_{DR}	Duplicates-removed sequence
S_{IC}	Compensated snapshot sequence
S_{RI}	Redundancy-increased sequence

assume each satellite node has the same fixed communication distance and all the satellites are located within the transmission range (determined by the fixed communication distance) of each other. Therefore, a satellite can reach all the other ones in one hop (directly). Based on the above assumptions, we can have $|\Omega_V| = N$ and $|\Omega_E| = \frac{1}{2}|\Omega_V|(|\Omega_V| - 1)$ where $|A|$ represents the cardinality, *i.e.*, the number of elements, of set A . The transmit power of each satellite is fixed to support the abovementioned communication distance.

That is, dynamic power control is not considered.

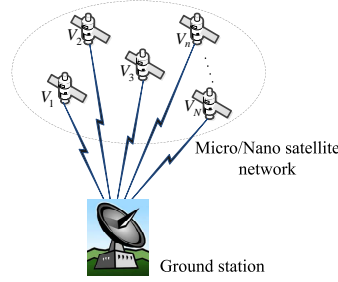


Fig. 2. System model.

We assume that dual-directional communication link can be established between arbitrary two nodes, *i.e.*, $E_{(V_i, V_j)} = E_{(V_j, V_i)}$ holds. Therefore, we can adopt, for simplicity, graph G as an undigraph to model the satellite network. The connection between different nodes in the network can be represented by an adjacency matrix \mathbf{A} as:

$$\mathbf{A} = \begin{bmatrix} E_{(V_1, V_1)} & \cdots & E_{(V_1, V_N)} \\ \vdots & \ddots & \vdots \\ E_{(V_N, V_1)} & \cdots & E_{(V_N, V_N)} \end{bmatrix}. \quad (2)$$

When $E_{(V_i, V_j)} = 1$, there exists link between nodes V_i and V_j ; otherwise, when $E_{(V_i, V_j)} = 0$, no connection exists between V_i and V_j . Note that the elements of main diagonal of \mathbf{A} are set to be 0, and since the links are nondirectional, \mathbf{A} is a symmetric matrix.

Fig. 2 plots the system model. As the figure shows, each micro/nano satellite maintains its own navigation information, including its position and speed in the reference system, and reports them to the ground station. The ground station collects the navigation data and failure probability of each micro/nano satellite, based on which topology control is carried out to generate a target topology. This topology control information is uploaded to all the satellite nodes. Then, each node sets up communication link according to the instructions.

The major parameters to be used in this paper are listed in Table 1.

3. DESIGN OF LOW-COST OFFLINE ICRTC

In this section, we will first propose the design of ICRTC method for topology control in mirco/nano satellite network, and then present a low-cost offline implementation of the method.

3.1 Design of ICRTC

The design of ICRTC algorithm is elaborated as follows. First, the ground station applies minimum spanning tree (MST) to the mirco/nano satellite network based on $G = (\Omega_V, \Omega_E)$ to obtain an initial topology $G_{Init} = (\Omega_{V, Init}, \Omega_{E, Init}^{MST})$. $\Omega_{V, Init} = \Omega_V$ holds. The value of the element in Ω_E is determined by the distance between each two corresponding satellite nodes. Note that the output of ICRTC, denoted by $G_{Tgt} = (\Omega_{V, Tgt}, \Omega_{E, Tgt})$, should

involve all N satellites in the network; that is, the target node set $\Omega_{V,Tgt}$ is the same as Ω_V and $\Omega_{V,Init}$. However, as for the link/edge set, according to the principle of ICRTC some links will be established to compensate for the fragile one(s) associated with the high-failure-probability nodes, hence we can have $\Omega_{E,Init}^{MST} \subset \Omega_{E,Tgt} \subset \Omega_E$. Specifically, $|\Omega_{E,Init}^{MST}| = |\Omega_V| - 1$ holds. We also define selected link set $\Omega_{E,\tau}$ in the τ th compensation. Then, we can get $\Omega_{E,\tau} = \Omega_{E,Init}^{MST}$ under $\tau = 0$.

In order to realize compensation, we first define a node-failure probability set as $P_V = \{p_{V_1}, \dots, p_{V_n}, \dots, p_{V_N}\}$ where p_{V_n} represents for the failure probability of satellite node V_n . The information of P_V is maintained at the ground station. If node V_i and V_j associate with link $E_{(V_i,V_j)}$, the link-failure probability of $E_{(V_i,V_j)}$ is $p_{E_{(V_i,V_j)}} = p_{V_i}(1 - p_{V_j}) + p_{V_j}(1 - p_{V_i}) + p_{V_i}p_{V_j} = p_{V_i} + p_{V_j} - p_{V_i}p_{V_j}$. Note that $p_{E_{(V_i,V_j)}} - 1 = (p_{V_i} - 1)(1 - p_{V_j}) \leq 0$, that is, $p_{E_{(V_i,V_j)}} \leq 1$ holds. We sort all satellites in descending order in terms of their node-failure probabilities to obtain a new node set, denoted by $\hat{\Omega}_V = \{\hat{V}_1, \dots, \hat{V}_n, \dots, \hat{V}_N\}$, for compensation. $p_{\hat{V}_1} > p_{\hat{V}_2} > \dots > p_{\hat{V}_n} > \dots > p_{\hat{V}_N}$ holds.

During the compensation, we employ two thresholds as the condition under which the algorithm terminates. The first one, denoted by ρ , is the maximum number of compensation times; the second one, η , is the target end-to-end transmission reliable probability. As for threshold ρ , we initialize the number of compensation times as $\tau = 0$. Each time when a node is selected from $\hat{\Omega}_V$ and compensated following ICRTC, we set $\tau \leftarrow \tau + 1$. As long as $\tau < \rho$, the compensation is continued/repeated. As for the use of threshold η , we first present the calculation of end-to-end transmission reliable probability as follows. We define a satellite set $\Omega_V^* = \{V_1^*, \dots, V_m^*, \dots, V_M^*\}$, containing all the nodes with only one degree, *i.e.*, V_m^* connects only one node and acting as either source or destination. Any two of the nodes in Ω_V^* , say V_i^* and V_j^* ($V_i^* \neq V_j^*$), can form an end-to-end node-pair $\{V_i^*, V_j^*\}$. Then, there are $K = \frac{1}{2}M(M-1)$ end-to-end node-pairs in total. We define the end-to-end transmission reliable probability of a path from V_i^* to V_j^* after the τ th compensation as $\Phi_{\{V_i^*, (\xi_l), V_j^*\}, \tau}$ where $V_i^*, V_j^* \in \Omega_V^*$. $\{V_i^*, (\xi_l), V_j^*\}$ ($l = 1, \dots, \Psi$) represents for the l th path of node-pair $\{V_i^*, V_j^*\}$, the link set constituting such a path (excluding the links associated with V_i^* and V_j^*) is denoted as ξ_l . As for different l , links of ξ_l vary. By noting that a path from V_i^* to V_j^* consists of multiple links belonging to the selected link set $\Omega_{E,\tau}$, $\Phi_{\{V_i^*, (\xi_l), V_j^*\}, \tau}$ can be calculated by multiplying the reliable probabilities of all the links in $\Omega_{E,\tau}$ constituting the path from V_i^* to V_j^* with each other. Since there may be multiple paths from V_i^* to V_j^* , we employ $\Phi_{\{V_i^*, V_j^*\}, \tau}$ to indicate the end-to-end transmission reliable probability of node-pair $\{V_i^*, V_j^*\}$ after the τ th compensation. The detailed discussion will be given in Section 4.

The compensation is realized in an iterative way. In each iteration, τ is at first updated to $\tau + 1$. On condition that $\tau < \rho$, the satellite node \hat{V}_τ in set $\hat{\Omega}_V$ is chosen for the τ th compensation. We define $\Omega_{V,\tau} = \Omega_V - \{\hat{V}_\tau\}$ and candidate edge set $\hat{\Omega}_{E,\tau} = \{E_{(V_i,V_j)}\}$ where $V_i, V_j \in \Omega_{V,\tau}$. That is, edges connected to \hat{V}_τ are removed from Ω_E . We can get $|\hat{\Omega}_{E,\tau}| = \frac{1}{2}|\Omega_{V,\tau}|(|\Omega_{V,\tau}| - 1)$. Then, we apply MST to graph $G_\tau = (\Omega_{V,\tau}, \hat{\Omega}_{E,\tau})$ to obtain a new topology whose selected link set is $\Omega_{E,\tau}^{MST} = \{E_{(V_i,V_j)}\}$ where $V_i, V_j \in \Omega_{V,\tau}$. $|\Omega_{E,\tau}^{MST}| = |\Omega_{V,\tau}| - 1$ and $\Omega_{E,\tau}^{MST} \subset \hat{\Omega}_{E,\tau}$ hold. In each compensation, the selected link set $\Omega_{E,\tau}$ is updated in terms of $\Omega_{E,\tau} \leftarrow \Omega_{E,\tau-1} \cup \Omega_{E,\tau}^{MST}$. That is, the compensation links ob-

tained under the assumption that node \hat{V}_τ is failure are added to the previous selected link set $\Omega_{E,\tau-1}$ to get the τ th compensated selected link set $\Omega_{E,\tau}$. In the beginning, *i.e.*, under $\tau = 0$, we have $\Omega_{E,\tau} = \Omega_{E,\tau}^{MST} = \Omega_{E,Init}^{MST}$. Upon obtaining $\Omega_{E,\tau}$, we re-calculate the end-to-end transmission reliable probability of the network, *i.e.*, $\Phi_{\{V_i^*, V_j^*\}, \tau}$, based on $\Omega_{E,\tau}$. If $\Phi_{\{V_i^*, V_j^*\}, \tau} < \eta$ and $\tau < \rho$, the compensation is repeated; otherwise, output target topology graph $G_{Tgt} = (\Omega_{V,Tgt}, \Omega_{E,Tgt})$ where $\Omega_{V,Tgt} = \Omega_V$ and $\Omega_{E,Tgt} = \Omega_{E,\tau}$, and ICRTC terminates.

Based on the above descriptions, we present the flowchart of ICRTC in Fig. 3 below.

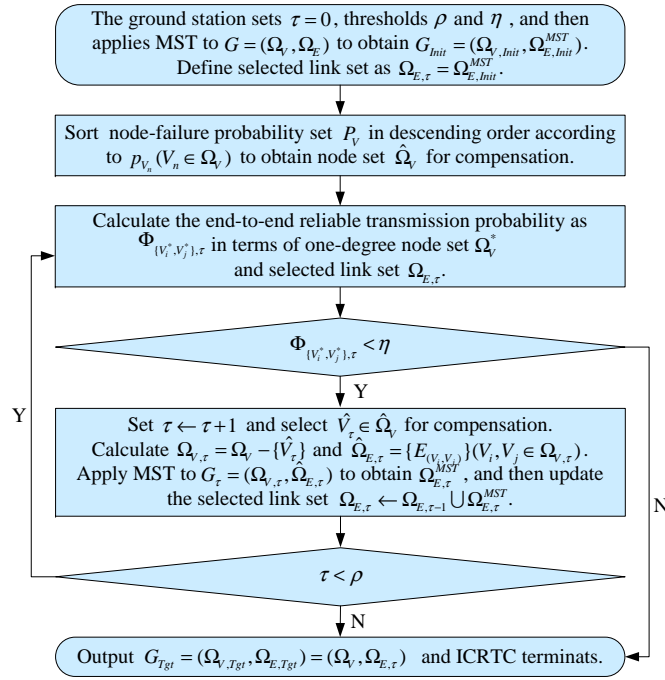


Fig. 3. Flowchart of ICRTC.

4. ANALYSIS OF END-TO-END TRANSMISSION RELIABLE PROBABILITY

Before delving into detailed analysis of end-to-end transmission reliable probability $\Phi_{\{V_i^*, V_j^*\}, \tau}$ after the τ th compensation, we first present the possible situations of compensation link(s) w.r.t. the high-failure-probability node \hat{V}_τ .

Without loss of generality, we employ V_S^* and V_D^* to denote the end points of an end-to-end path determined by node-pair $\{V_S^*, V_D^*\}$. Both V_S^* and V_D^* belong to set $\Omega_{\hat{V}_\tau}$. We assume the path from V_S^* to V_D^* is via a high-failure-probability node \hat{V}_τ . Since MST is applied to $G_\tau = (\Omega_{V,\tau}, \hat{\Omega}_{E,\tau})$ where $\Omega_{V,\tau} = \Omega_V - \{\hat{V}_\tau\}$ and $\hat{\Omega}_{E,\tau} = \{E_{(V_i, V_j)}\}$

($V_i, V_j \in \Omega_{V,\tau}$), the obtained $G_\tau^{MST} = (\Omega_{V,\tau}, \Omega_{E,\tau}^{MST})$ doesn't contain cyclic. As shown in Fig. 4, the path from V_S^* and V_D^* can be represented by the following node sequence $\{V_S^*, \dots, V_{a_2}, V_{a_1}, \dots, V_{a_0}, \hat{V}_\tau, V_{b_0}, \dots, V_{b_1}, V_{b_2}, \dots, V_D^*\}$. Before the τ th compensation, when node \hat{V}_τ fails, the two links/edges $E_{(V_a, \hat{V}_\tau)}$ and $E_{(\hat{V}_\tau, V_b)}$ in Fig. 3 become disconnected, thus separating areas A from B.

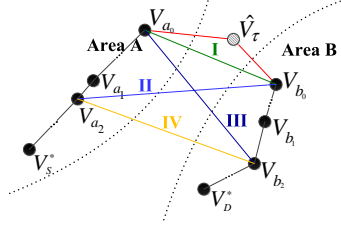


Fig. 4. Illustration of various situations of compensation links with ICRTC.

In the τ th compensation, MST is applied to $G_\tau = (\Omega_{V,\tau}, \hat{\Omega}_{E,\tau})$ where $\Omega_{V,\tau} = \Omega_V - \{\hat{V}_\tau\}$ and $\hat{\Omega}_{E,\tau} = \{E_{(V_i, V_j)}\}$ ($V_i, V_j \in \Omega_{V,\tau}$). The compensation link determined by ICRTC can be one of four situations, indexed by I, II, III and IV, respectively, in Fig. 4. In case of I, $E_{(V_{a_0}, V_{b_0})}$ is added to the selected link set $\Omega_{E,\tau}$ (both V_{a_0} and V_{b_0} are \hat{V}_τ 's one-hop neighboring nodes). Then a compensation path $\{V_S^*, \dots, V_{a_2}, V_{a_1}, \dots, V_{a_0}, V_{b_0}, \dots, V_{b_1}, V_{b_2}, \dots, V_D^*\}$ becomes available. Similarly, in situations II and III, the compensation links are $E_{(V_{a_2}, V_{b_0})}$ and $E_{(V_{a_0}, V_{b_2})}$, respectively. In these two cases, only one end of the compensation link is \hat{V}_τ 's one-hop neighboring node whereas the other end lies in either area A (case II) or B (case III) — we employ V_{a_2} (case II) and V_{b_2} (case III), both of which reach \hat{V}_τ via multi-hop links, in Fig. 4 as an example. In case of IV, both ends of the compensation link reach \hat{V}_τ via multi-hop links. In Fig. 4, we plot $E_{(V_{a_2}, V_{b_2})}$ as an example of case IV. For simplicity, we don't give the compensation paths of cases II, III and IV. Then, $\Phi_{\{V_S^*, V_D^*\}, \tau}$ can be calculated following the descriptions in Section 3.

It should be noted that in evaluating network's end-to-end transmission reliable probability, both the paths from V_S^* via \hat{V}_τ and through the compensation link(s) to V_D^* need to be taken into account. For simplicity, we use $\{V_S^*, (\hat{V}_\tau), V_D^*\}$ to denote the end-to-end path via \hat{V}_τ ; similarly, $\{V_S^*, (V_a^{\mathcal{M}}, V_b^{\mathcal{M}}), V_D^*\}$ represents for the path via compensation link associated with node $V_a^{\mathcal{M}}$ in area A and $V_b^{\mathcal{M}}$ in area B where the superscript $\mathcal{M} \in \{I, II, III, IV\}$ denotes different compensation situations. For example, when $\mathcal{M} = I$, we have $V_a^I = V_{a_0}$ and $V_b^I = V_{b_0}$ as shown in Fig. 4. Without ambiguity, we also use $\{V_S^*, (\hat{V}_\tau), V_D^*\}$ and $\{V_S^*, (V_a^{\mathcal{M}}, V_b^{\mathcal{M}}), V_D^*\}$ to denote the node sets constituting corresponding paths. Then, the end-to-end transmission reliable probability via the above two types of paths can be calculated as follows:

$$\Phi_{\{V_S^*, (\hat{V}_\tau), V_D^*\}, \tau} = \prod_{V_i, V_j \in \{V_S^*, (\hat{V}_\tau), V_D^*\}} [1 - pE_{(V_i, V_j)}] \quad (3)$$

$$\Phi_{\{V_S^*, (V_a^{\mathcal{M}}, V_b^{\mathcal{M}}), V_D^*\}, \tau} = \prod_{V_i, V_j \in \{V_S^*, (V_a^{\mathcal{M}}, V_b^{\mathcal{M}}), V_D^*\}} [1 - pE_{(V_i, V_j)}] \quad (4)$$

where \prod means computing the product of reliable probabilities of all the one-hop links $E_{(V_i, V_j)}$ (that is, V_i and V_j should be neighboring nodes). V_i and V_j belong to either the

node set $\{V_S^*, (\hat{V}_\tau), V_D^*\}$ in Eq. (1) or $\{V_S^*, (V_a^M, V_b^M), V_D^*\}$ in Eq. (2). According to $P(A \cup B) = P(A) + P(B) - P(A \cap B)$ where $P(A)$ and $P(B)$ represents the probabilities that event A and B occur, respectively, $P(A \cup B)$ denotes the probability that A or B happens, and $P(A \cap B)$ is the probability that both A and B occur simultaneously. Then, the end-to-end transmission reliable probability of node-pair $\{V_S^*, V_D^*\}$ can be calculated as:

$$\begin{aligned} \Phi_{\{V_S^*, V_D^*\}, \tau} &= \Phi_{\{V_S^*, (\hat{V}_\tau), V_D^*\}, \tau} + \Phi_{\{V_S^*, (V_a^M, V_b^M), V_D^*\}, \tau} \\ &\quad - \Phi_{\{V_S^*, (\hat{V}_\tau), V_D^*\}, \tau} \Phi_{\{V_S^*, (V_a^M, V_b^M), V_D^*\}, \tau} \end{aligned} \quad (5)$$

After the τ th compensation, there may be multiple paths between V_i^* and V_j^* where $V_i^*, V_j^* \in \Omega_V^*$ and $V_i^* \neq V_j^*$. Defining the number of possible paths between node-pair $\{V_i^*, V_j^*\}$ as Ψ , then the path set of node-pair $\{V_i^*, V_j^*\}$ can be written as $L_{\{V_i^*, V_j^*\}} = \{\{V_i^*, (\xi_l), V_j^*\}\}$ where $\{V_i^*, (\xi_l), V_j^*\}$ denotes a path between node-pair $\{V_i^*, V_j^*\}$ involving link set ξ_l (ξ_l contains the links constituting path $\{V_i^*, (\xi_l), V_j^*\}$ while excluding the links associated with the end nodes, *i.e.*, V_i^* and V_j^* , of the path). We can get $|L_{\{V_i^*, V_j^*\}}| = \Psi$. So, the end-to-end transmission reliable probability of node-pair $\{V_i^*, V_j^*\}$ after the τ th compensation can be computed as:

$$\begin{aligned} \Phi_{\{V_i^*, V_j^*\}, \tau}^{[\Psi]} &= (-1)^0 \sum_{l=1}^{\Psi} \Phi_{\{V_i^*, (\xi_l), V_j^*\}, \tau} \\ &\quad + (-1)^1 \sum_{l=1}^{\Psi-1} \sum_{m=l+1}^{\Psi} \Phi_{\{V_i^*, (\xi_l), V_j^*\}, \tau} \Phi_{\{V_i^*, (\xi_m), V_j^*\}, \tau} \\ &\quad + (-1)^2 \sum_{l=1}^{\Psi-2} \sum_{m=l+1}^{\Psi-1} \sum_{q=l+2}^{\Psi} \Phi_{\{V_i^*, (\xi_l), V_j^*\}, \tau} \Phi_{\{V_i^*, (\xi_m), V_j^*\}, \tau} \Phi_{\{V_i^*, (\xi_q), V_j^*\}, \tau} \\ &\quad + \dots + (-1)^{\Psi-1} \prod_{l=1}^{\Psi} \Phi_{\{V_i^*, (\xi_l), V_j^*\}, \tau} \end{aligned} \quad (6)$$

Eq. (6) can be proved by using *mathematical induction*. The details are given in Appendix A.

The above discussions about Fig. 4 consider one-time compensation w.r.t. a high-failure-probability node \hat{V}_τ . However, in practical use, multiple times of compensation may be required. Fortunately, based on the principle of ICRTC, the above evaluation of end-to-end transmission reliable probability can be directly extended to the case of multiple times of compensation. This is because in a compensation, say indexed by τ , MST is applied to $G_\tau = (\Omega_{V, \tau}, \hat{\Omega}_{E, \tau})$ where $\Omega_{V, \tau} = \Omega_V - \{\hat{V}_\tau\}$ and $\hat{\Omega}_{E, \tau} = \{E_{(V_i, V_j)}\} (V_i, V_j \in \Omega_{V, \tau})$, to obtain $G_\tau^{MST} = (\Omega_{V, \tau}, \Omega_{E, \tau}^{MST})$; and then the selected link set $\Omega_{E, \tau}$ is updated in terms of $\Omega_{E, \tau} \leftarrow \Omega_{E, \tau-1} \cup \Omega_{E, \tau}^{MST}$. Therefore, the compensation is independent from each other. For example, when two successive compensations are considered, say indexed by τ and $\tau+1$, respectively, since in each compensation there is 4 possible situations of the compensation links w.r.t. each of the high-failure-probability nodes, *i.e.*, \hat{V}_τ and $\hat{V}_{\tau+1}$, there exist 16 situations in total in the case of two times of compensation. As Fig. 5 shows, we add subscript τ or $\tau+1$ to I, II, III and IV, to distinguish various compensation link situations in different compensations. It should be noticed that areas A and B are divided w.r.t. \hat{V}_τ whereas areas C and D are in terms of $\hat{V}_{\tau+1}$. That is, A and B (C and D) don't overlap with each other; however, A (or B) may overlap with C (or D).

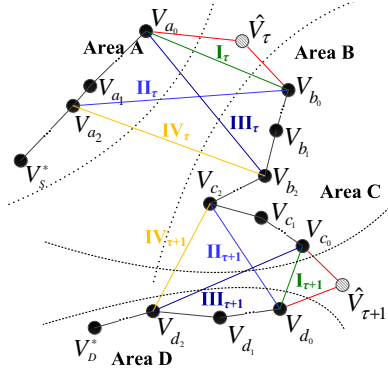


Fig. 5. Illustration of various situations of compensation links with ICRTC under two times of compensation.

5. LOW-COST OFFLINE IMPLEMENTATION OF ICRTC

In this section, we will present an offline implementation of the proposed ICRTC. At present, the offline topology control is mainly based on the analysis of snapshot sequence, with which a period of time is divided into multiple time intervals, named as time slots. In each slot, the network topology is regarded as unchanged and hence can be represented by a topology snapshot. In this way, real-time topology control is converted to a series of semi-static control. In practical use of micro/nano satellite network, the periodicity of orbiting satellites can be exploited to simplify the snapshot sequence, so that onboard storage for storing topology information can be saved. In what follows, we will first present the preprocess of snapshot sequence, and then propose a snapshot simplification strategy which can reduce the number of snapshots in the sequence by employing a few redundant links.

5.1 Preprocessing of Snapshot Sequence

The offline topology control can fully utilize the computational resource of ground station in accurately pre-calculating the topology in each time slot of the orbiting micro/nano satellite network. The length of time slot, denoted as Δt , affects the precision of offline topology control. The smaller the Δt , the more precise the topology is controlled and the better the variation of network environment can be adapted to; however, larger number of snapshots are generated and need to be stored in the satellite. Therefore, it is necessary to merge successive snapshots of the same topology in the snapshot sequence so as to reduce topology redundancy.

In order to achieve the above goal, we divide the slot-length Δt into *topology adjustment phase* t_ϕ and *topology maintaining phase* t_γ . The network topology is regarded unchanged in t_γ and can be used to represent a corresponding snapshot. When a micro/nano satellite network starts to adjust its topology, it first needs to establish or remove inter-satellite links in t_ϕ , and then in t_γ maintain the adjusted topology until the next time slot starts. Based on the above discussion, we can have:

$$\Delta t = t_\phi + t_\gamma. \quad (7)$$

Once Δt is determined, we can obtain a snapshot sequence, denote as S , and then preprocess S for later simplification. We consider a satellite network consisting of N nodes. First, we use Δt to divide the orbit period T in $\lceil T/\Delta t \rceil$ slots where $\lceil \cdot \rceil$ represents for rounding up to an integer. An arbitrary slot is indexed by ε where $\varepsilon \in \{0, 1, \dots, \lceil T/\Delta t \rceil\}$. Then, in each time slot, we calculate the Euclidean distance $d_{i,j}$ ($i \neq j$ and $i, j \in \{1, \dots, N\}$) between nodes V_i and V_j . The results in slot ε can be represented by an $N \times N$ distance matrix \mathbf{D}_ε . We use \mathbf{D}_ε as the input of the MST algorithm to obtain a topology snapshot s_ε at time instant t_ε which is the starting point of a time slot. The topology of network in a slot starting from t_ε can thus be represented by an $N \times N$ adjacency matrix \mathbf{A}_ε . Finally, we successively check all of the snapshots in sequence S and combine those of the same topology; in this way S can be simplified to a new *duplicates-removed sequence*, denoted as S_{DR} .

5.2 Redundancy-Increasing Based Snapshot Sequence Simplification

Upon obtaining S_{DR} , we apply ICRTC to each of the snapshots in S_{DR} so as to enhance the robustness of network. Then, we can get a compensated snapshot sequence, denoted as S_{IC} . Although most of the successive snapshots in S_{IC} after applying ICRTC may have various topologies, adjacent snapshots may have similar topologies, *i.e.*, only a few links in successive snapshots are different. Therefore, we can merge adjacent similar snapshots by employing a few redundant links so that redundancy of S_{IC} can be further reduced.

To realize redundancy-increasing based simplification, we first calculate $\mathbf{Q}_\varepsilon = \mathbf{A}_\varepsilon \oplus \mathbf{A}_\phi$ where \mathbf{A}_ε and \mathbf{A}_ϕ are adjacent matrices corresponding to two successive topology snapshots s_ε and s_ϕ in S_{IC} , respectively. \oplus is bit-wise exclusive OR (XOR) operation. Then, we can have the Frobenius norm of \mathbf{Q}_ε as $\|\mathbf{Q}_\varepsilon\|_F = (\sum_{i=1}^N \sum_{j=1}^N \sigma_{i,j}^2)^{1/2}$ where $\sigma_{i,j}$ is the element in the i th row and j th column of matrix \mathbf{Q}_ε . $\|\mathbf{Q}_\varepsilon\|_F$ indicates the number of element 1 in \mathbf{Q}_ε . Then, we can adopt $\frac{1}{2}\|\mathbf{Q}_\varepsilon\|_F$ as the indication of topology difference of snapshots s_ε and s_ϕ . If $\frac{1}{2}\|\mathbf{Q}_\varepsilon\|_F < \varphi$ where φ is a pre-defined threshold indicating the degree of dissimilarity of two snapshots, snapshots s_ε and s_ϕ have similar topologies, so that we can add redundant links to s_ε and s_ϕ according to the indices of elements 1 in \mathbf{Q}_ε . Then, \mathbf{A}_ε and \mathbf{A}_ϕ are updated according to $\mathbf{A}_\varepsilon \leftarrow \mathbf{A}_\varepsilon \oplus \mathbf{Q}_\varepsilon$ and $\mathbf{A}_\phi \leftarrow \mathbf{A}_\phi \oplus \mathbf{Q}_\varepsilon$, respectively. Note that since the updated \mathbf{A}_ε and \mathbf{A}_ϕ are identical, we delete snapshot s_ϕ from sequence S_{IC} and update the sequence as $S_{IC} \leftarrow S_{IC} - \{s_\phi\}$.

For example, given $\mathbf{A}_\varepsilon = \begin{pmatrix} 0 & 1 & 0 & 0 \\ 1 & 0 & 1 & 0 \\ 0 & 1 & 0 & 1 \\ 0 & 0 & 1 & 0 \end{pmatrix}$ and $\mathbf{A}_\phi = \begin{pmatrix} 0 & 1 & 0 & 0 \\ 1 & 0 & 1 & 1 \\ 0 & 1 & 0 & 0 \\ 0 & 1 & 0 & 0 \end{pmatrix}$, we can have

$\mathbf{Q}_\varepsilon = \mathbf{A}_\varepsilon \oplus \mathbf{A}_\phi = \begin{pmatrix} 0 & 0 & 0 & 0 \\ 0 & 0 & 0 & 1 \\ 0 & 0 & 0 & 1 \\ 0 & 1 & 1 & 0 \end{pmatrix}$ and $\frac{1}{2}\|\mathbf{Q}_\varepsilon\|_F = 2$. We let $\varphi = 3$, then both \mathbf{A}_ε and \mathbf{A}_ϕ

are updated to $\mathbf{A}_\varepsilon = \mathbf{A}_\phi = \begin{pmatrix} 0 & 1 & 0 & 0 \\ 1 & 0 & 1 & 1 \\ 0 & 1 & 0 & 1 \\ 0 & 1 & 1 & 0 \end{pmatrix}$ by adding link $E_{(v_2, v_4)}$ to s_ε and $E_{(v_3, v_4)}$ to

s_ϕ , respectively. After checking all of the snapshots in S_{IC} and combining similar ones, we can get a simplified *redundancy-increased sequence* S_{RI} .

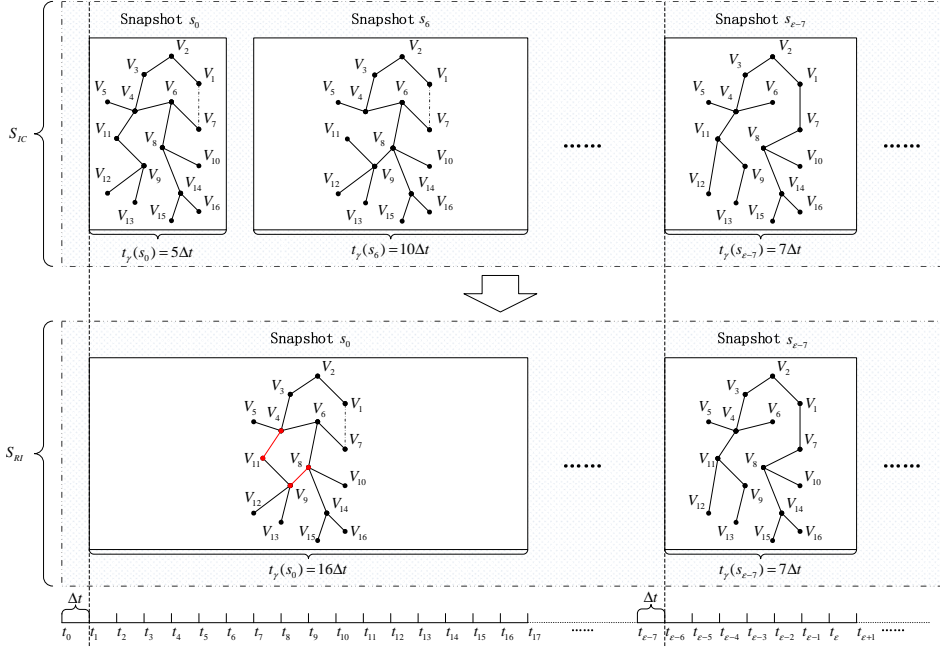


Fig. 6. Illustration of redundancy-increasing based simplification.

Fig. 6 illustrates the principle of redundancy-increasing based snapshot sequence simplification. As the figure shows, after applying ICRTC to all of the snapshots in S , we have S_{IC} . The dotted line represents for the compensation link ($E_{(V_1, V_7)}$) in snapshots s_0 and s_6) determined in terms of ICRTC. By comparison of s_0 and s_6 , we can see that there are two different links, *i.e.*, $E_{(V_4, V_{11})}$ and $E_{(V_8, V_9)}$. Then, by adding redundant links $E_{(V_4, V_{11})}$ and $E_{(V_8, V_9)}$ (which are colored red) and s_0 , respectively, we can merge s_0 and s_6 in S_{IC} into s_0 in S_{RI} . By doing so, the topology maintaining phase of s_0 in S_{RI} becomes $t_\gamma(s_0) = 16\Delta t$, while as a comparison, in sequence S_{DR} , $t_\gamma(s_0) = 5\Delta t$ and $t_\gamma(s_6) = 10\Delta t$. That is, by employing a few redundant links, we can maintain the network topology without adjustment for a longer time, and hence reducing the cost for adjusting the connections between network nodes.

6. SIMULATION RESULTS

In this section, we use STK (System Tool Kit) and MATLAB to simulate the proposed topology control algorithm and its implementation. The STK software is developed by AGI (Analytical Graphics, Inc.) for modeling, analysis and demonstration of space missions and defense systems. First, we jointly use MATLAB and STK to demonstrate an orbiting micro/nano satellite network. We consider $N = 16$ satellite nodes. The Kepler orbital elements are given in Table 2 below.

Table 2. Kepler orbital elements settings of micro/nano satellites.

Parameter	Value	Random offset range
a (km)	7800	± 10
θ ($^\circ$)	95	± 3
Ω ($^\circ$)	275	± 3
ω ($^\circ$)	175	± 3
M ($^\circ$)	180	± 3
e ($^\circ$)	0	0

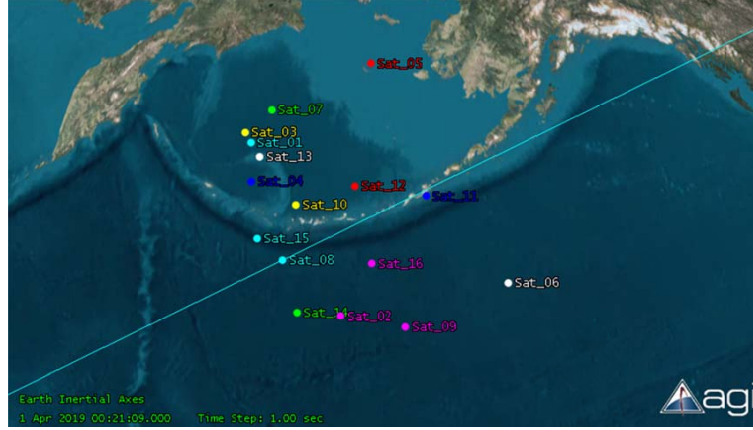


Fig. 7. Demonstration of micro/nano satellite network.

We set simulation duration to be 60 minutes and adopt $\Delta t = 1s$. The above parameters are generated in MATLAB and then transferred to STK via a STK–MATLAB connector so that the orbiting micro/nano satellite network in space environment can be demonstrated.

Fig. 7 shows 16 micro/nano satellites scattering in their orbits. The distance between two satellite nodes ranges from 100km–1000km. As the relative positions of all satellites vary with time, the topology of the satellite network also dynamically changes.

Next, we use MATLAB simulation to evaluate the performance of ICRTC. We also simulate MST without compensation and another method called traceable compensation based robust topology control (TCRTC) [28] for comparison. Similarly to ICRTC, TCRTC works in an iterative way. TCRTC works in an iterative way similarly to the proposed ICRTC. TCRTC first generates a simply connected MST topology, represented by graph $G_{Init} = (\Omega_{V,Init}^{MST}, \hat{\Omega}_{E,Init}^{MST})$ where $\Omega_{V,Init}^{MST} = \Omega_V$, by using MST, and then compensates multiple satellites with the highest failure probabilities. The number of compensated satellites is the same as that of the compensation time τ . Although the $\tau - 1$ high-failure-probability satellites, *i.e.*, $\hat{V}_{\tau-1}, \dots, \hat{V}_1$, are compensated together with node \hat{V}_τ in the τ th compensation, only the link set $\Omega_{E,\tau}^{MST}$ is used for compensating $\Omega_{E,Init}^{MST}$ whereas $\Omega_{E,\tau-1}^{MST}, \dots, \Omega_{E,1}^{MST}$ are discarded. Specifically, in the first compensation ($\tau = 1$), TCRTC is realized the same as ICRTC, whereas in the following compensation ($\tau > 1$), TCRTC applies MST to $G_\tau = (\Omega_{V,\tau}, \hat{\Omega}_{E,\tau})$ where $\Omega_{V,\tau} = \Omega_V - \{\hat{V}_\tau, \hat{V}_{\tau-1}, \dots, \hat{V}_1\}$ and $\hat{\Omega}_{E,\tau} = \{E_{(V_i, V_j)}\}$ ($V_i, V_j \in \Omega_{V,\tau}$) to obtain $G_\tau^{MST} = (\Omega_{V,\tau}, \Omega_{E,\tau}^{MST})$. Then, the selected link set $\Omega_{E,\tau}$ is updated in terms of

$\Omega_{E,\tau} \leftarrow \Omega_{E,\tau}^{MST} \cup \Omega_{E,Init}^{MST}$. As for MST which is a well-known method [29], its descriptions are as follows. Given a connected and undirected graph $G = (\Omega_V, \Omega_E)$ where Ω_V denotes the node set and Ω_E is the link/edge set indicating possible interconnections between node-pairs, we assume a weight $\varpi[E_{(V_i,V_j)}]$ is associated with each link $E_{(V_i,V_j)}$ specifying the cost for connecting nodes V_i and V_j . We can then find an acyclic subset $\Omega_E^{MST} \subseteq \Omega_E$ that connects all of the nodes in Ω_V and yields the minimum total weight $\varpi(\Omega_E^{MST}) = \sum_{E_{(V_i,V_j)} \in \Omega_E^{MST}} \varpi[E_{(V_i,V_j)}]$. We call Ω_E^{MST} the *minimum spanning tree*.

The parameter settings are given in Table 3 as below. We consider a 50km×50km area. Then, $N = 10$ micro/nano satellite nodes are randomly and uniformly generated in this area. Node-failure probability is randomly selected within region $(0,1)$. The value/weight of an edge $E_{(V_i,V_j)}$ is determined by the physical distance between nodes V_i and V_j . For simplicity, at most two times of compensation are taken into account, *i.e.*, $\rho \in \{1,2\}$. In the simulation of Figs. 8 and 9, we set $\eta = 0.5$, whereas for Figs. 10 and 11, since we focus on the influence of the number of compensation times on the end-to-end transmission reliable probability, we don't use η in the simulation (denoted by “-” in Table 3).

Table 3. Parameter settings for ICRTC simulation.

Parameter	Value
Area	50km×50km
N	10
ρ	{1,2}
η	{0.5,-}
P_{V_n}	(0,1)

We first verify the effectiveness of the proposed ICRTC by simulating and showing its working process in Fig. 8. As the figure shows, the network contains $N = 10$ nodes. $\Omega_{V,\tau} = \{V_1, \dots, V_{10}\}$. Under the assumption that any satellite node is capable of communicating with all the other nodes, we can have the candidate link/edge set $\hat{\Omega}_{E,\tau} = \{E_{(V_i,V_j)}\}$ where $V_i, V_j \in \Omega_{V,\tau}$ and $|\hat{\Omega}_{E,\tau}| = \frac{1}{2}|\Omega_{V,\tau}|(|\Omega_{V,\tau}| - 1) = 45$. As shown in Fig. 8 (a), the selected link set obtained after applying MST under $\tau = 0$ is $\Omega_{E,Init}^{MST} = \{E_{(V_1,V_5)}, E_{(V_1,V_2)}, E_{(V_2,V_6)}, E_{(V_6,V_7)}, E_{(V_6,V_8)}, E_{(V_8,V_4)}, E_{(V_8,V_3)}, E_{(V_3,V_{10})}, E_{(V_{10},V_9)}\}$. In this experiment, the randomly generated node failure probability set is $P_V = \{0.174, 0.386, 0.304, 0.274, 0.198, 0.433, 0.371, 0.005, 0.064, 0.217\}$. Sorting all the satellites in descending order based on their fault probabilities, we have $\hat{\Omega}_V = \{V_6, V_2, V_7, V_3, V_4, V_{10}, V_5, V_1, V_9, V_8\}$. By observing Fig. 8 (a), we can get the one-degree node set $\Omega_V^* = \{V_4^*, V_5^*, V_7^*, V_9^*\}$ ($M = |\Omega_V^*| = 4$). Then, there are $\frac{1}{2}M(M-1) = 6$ end-to-end node-pairs in total; they are $\{V_4^*, V_5^*\}$, $\{V_4^*, V_7^*\}$, $\{V_4^*, V_9^*\}$, $\{V_5^*, V_7^*\}$, $\{V_5^*, V_9^*\}$ and $\{V_7^*, V_9^*\}$.

Fig. 8 (b) plots the network topology of graph $(\Omega_{V,1}, \Omega_{E,1}^{MST})$ in the first compensation ($\tau = 1$). As the figure shows, $\hat{V}_1 = V_6$ is selected for the first compensation. We can have $\Omega_{V,1} = \Omega_V - V_6$, $\hat{\Omega}_{E,1} = \{E_{(V_i,V_j)}\}$ ($V_i, V_j \in \Omega_{V,1}$), and $|\hat{\Omega}_{E,1}| = \frac{1}{2}|\Omega_{V,1}|(|\Omega_{V,1}| - 1) = 36$. So, after applying MST to $G_1 = (\Omega_{V,1}, \hat{\Omega}_{E,1})$, we get $\Omega_{E,1}^{MST} = \{E_{(V_1,V_5)}, E_{(V_1,V_2)}, E_{(V_2,V_7)}, E_{(V_2,V_8)}, E_{(V_8,V_4)}, E_{(V_8,V_3)}, E_{(V_3,V_{10})}, E_{(V_{10},V_9)}\}$, as plotted in Fig. 8 (b). The compensation links are $E_{(V_2,V_7)}$ and $E_{(V_2,V_8)}$.

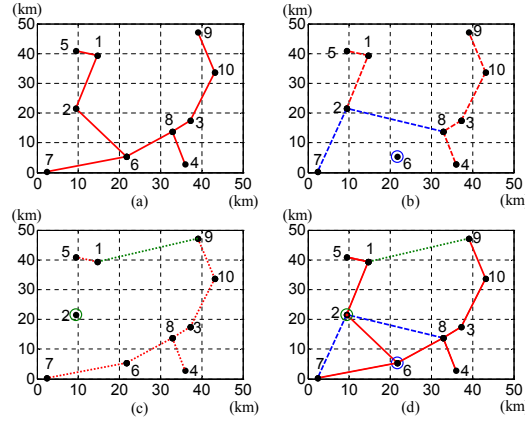

 Fig. 8. Illustration of the operation of ICRTC under $\tau = 2$.

Fig. 8 (c) shows the network topology of graph $(\Omega_{V,2}, \Omega_{E,2}^{MST})$ in the second compensation. Similarly to the operation in Figs. 8 (b), in Fig. 8 (c), $\Omega_{V,2} = \Omega_V - V_2$ and $\hat{\Omega}_{E,2} = \{E_{(V_i, V_j)}\}$ ($V_i, V_j \in \Omega_{V,2}$). Then, after applying MST to $G_2 = (\Omega_{V,2}, \hat{\Omega}_{E,2})$, we get $\Omega_{E,2}^{MST} = \{E_{(V_6, V_7)}, E_{(V_6, V_8)}, E_{(V_8, V_4)}, E_{(V_8, V_3)}, E_{(V_3, V_{10})}, E_{(V_{10}, V_9)}, E_{(V_1, V_9)}, E_{(V_1, V_5)}\}$. The compensation link is $E_{(V_1, V_9)}$.

In Fig. 8 (d), we plot the network topology of graph $(\Omega_{V,2}, \Omega_{E,2}^{MST})$, *i.e.*, $G_{Tgt} = (\Omega_{V, Tgt}, \Omega_{E, Tgt})$ after the second compensation. We can see that for $\tau = 1$, we add links $E_{(V_2, V_7)}$ and $E_{(V_2, V_8)}$ (blue dashed lines) to the initial selected link set $\Omega_{E, Init}^{MST}$ to obtain $\Omega_{E,1}$, *i.e.*, $\Omega_{E,1} \leftarrow \Omega_{E, Init}^{MST} \cup \Omega_{E,1}^{MST}$. Similarly, after the second compensation, $E_{(V_1, V_9)}$ (green dotted line) is added as a backup link w.r.t. V_2 to $\Omega_{E,1}$. That is, $\Omega_{E,2} \leftarrow \Omega_{E,1} \cup \Omega_{E,2}^{MST}$.

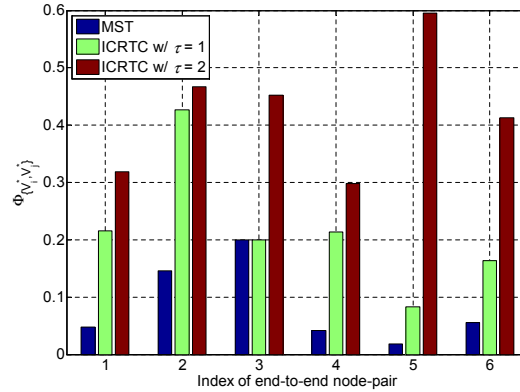


Fig. 9. End-to-end transmission reliable probabilities of various node-pairs.

In Fig. 9, we plot the end-to-end transmission reliable probability of each node-pair in Ω_V^* with various methods in one experiment. The numbers on x-axis indicate the indices of end-to-end node-pairs. The parameter settings in this experiment are the same as those in Fig. 8. Since there are 4 nodes in Ω_V^* , *i.e.*, $\Omega_V^* = \{V_4^*, V_5^*, V_7^*, V_9^*\}$, six node-pairs,

i.e., $\{V_4^*, V_5^*\}$, $\{V_4^*, V_7^*\}$, $\{V_4^*, V_9^*\}$, $\{V_5^*, V_7^*\}$, $\{V_5^*, V_9^*\}$ and $\{V_7^*, V_9^*\}$ indexed by 1, 2, 3, 4, 5 and 6, respectively, exist. As the figure shows, the end-to-end transmission reliable probability of a node-pair doesn't fall as τ increases. In some situations, compensation may not yield the increase of reliability performance. This is because in such cases there is no high-failure-probability node in the path of the investigated node-pair, incurring the compensation doesn't improve the end-to-end reliable probability. For example, in the compensation of node-pair $\{V_4^*, V_9^*\}$ indexed by 3 as shown in Fig. 9. In the first compensation, the backup links $E_{(V_2, V_7)}$ and $E_{(V_2, V_8)}$ don't contribute to the improvement of transmission reliable probability from V_4^* to V_9^* ; while in the second compensation, new paths $\{V_4^*, V_8, V_2, V_1, V_9^*\}$, $\{V_4^*, V_8, V_6, V_2, V_1, V_9^*\}$, and $\{V_4^*, V_8, V_6, V_7, V_2, V_1, V_9^*\}$ become available in addition to the original end-to-end path $\{V_4^*, V_8, V_3, V_{10}, V_9^*\}$, hence significantly improving the end-to-end robustness of node-pair $\{V_4^*, V_9^*\}$. It should be noticed that in the simulation of Figs. 8 and 9, although $\Phi_{\{V_i^*, V_j^*\}, 2}$ is not as large as $\eta = 0.5$, since τ has reached the threshold $\rho = 2$, ICRTC should terminate. In practice, one can adopt a larger ρ to realize good enough end-to-end reliable performance.

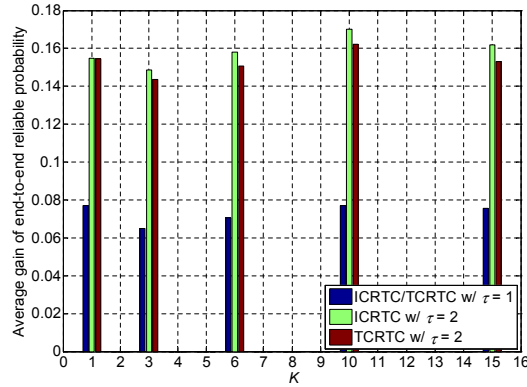


Fig. 10. Average gain of network's end-to-end transmission reliable probability with different methods under various K s.

Fig. 10 shows the average gain of network's end-to-end transmission reliable probability under various methods compared with MST. Monte-Carlo simulation is employed where the average is over 2.5×10^4 samples. We consider $N = 10$ satellite nodes and $M \in \{2, 3, 4, 5, 6\}$ one-degree nodes in each experiment. It should be noticed that although M can be as large as 9, *i.e.*, star topology, since the probability of more than 6 one-degree nodes exist is extremely small, we omit the case of $M \in \{7, 8, 9\}$ in the experiment. Under $M \in \{2, 3, 4, 5, 6\}$, we can have the number of one-degree node-pairs $K = \frac{1}{2}M(M-1) \in \{1, 3, 6, 10, 15\}$. As shown in Fig. 10, under $\tau = 1$, the operation of ICRTC is the same as that of TCRTC. The performance gain with one-time compensation is inferior to that with two times of compensation. Under $\tau = 2$, the performance gain of ICRTC excels that of TCRTC. Fig. 11 plots the average link redundancy cost of various methods compared with MST. The average is over 2.5×10^4 samples. The x-axis is the same as that of Fig. 10. Link redundancy cost is defined as the number of links added to $\Omega_{E, Init}^{MST}$. As the figures shows, under $\tau = 2$, ICRTC yields the highest link cost of all three cases. That is, compared to TCRTC, ICRTC yields higher end-to-end reliable

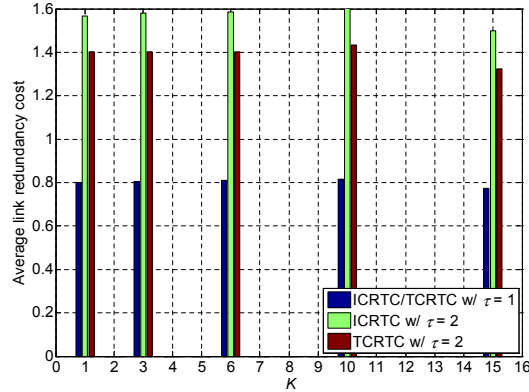


Fig. 11. Average link redundancy cost with different methods under various K s.

performance gain (see in Fig. 10) at the cost of more redundant link overhead. However, by noting that TCRTC realizes compensation by canceling all the backup link(s) calculated in the previous compensation(s), the network's end-to-end reliable probability may reduce as τ grows, incurring the requirement of an inspecting logic to determine whether further compensation is necessary. As a comparison, ICRTC's end-to-end reliability monotonously improves with an increase of τ as shown in Fig. 9. For space limit, we don't give the result here.

Finally, we will evaluate the performance of the low-cost offline implementation of ICRTC. In the simulation, we take various N and φ to study their influence on the simplification efficiency of the strategy proposed in Section 5. Let $|S|$ be the number of snapshots in initial sequence S . Then, $|S_{DR}|$ is the number of snapshots in sequence S_{DR} , and $|S_{RI}|$ denotes the number of snapshots in sequence S_{RI} . So, the simplification efficiency of duplicates-removal (DR) and redundancy-increasing (RI) can be defined as $\alpha = \frac{|S|-|S_{DR}|}{|S|}$ and $\beta = \frac{|S|-|S_{RI}|}{|S|}$, respectively. We also simulate equal time slot dividing [21] for comparison. We use $S_{ED}(\Delta t)$ to denote the simplified snapshot sequence obtained by equally dividing the orbit period T with time interval Δt . It should be noticed that when $\Delta t = 1$ s, $S_{ED}(\Delta t)$ becomes the initial sequence S . Similarly, we can define $\chi(\Delta t) = \frac{|S|-|S_{ED}(\Delta t)|}{|S|}$ to indicate the simplification efficiency of equal dividing.

Fig. 12 shows the variation of simplification efficiency with N under $\varphi = 3$. N is selected from set $\{8, 16, 32, 64\}$. We employ Monte-carlo simulation to obtain the average efficiency performance. As the figure shows, β outperforms α , indicating that by adding a few redundant links, the cost for topology control (*i.e.*, the number of snapshots) can be effectively reduced. Moreover, both α and β decrease as N grows. This is because given the same number of topology snapshots, the number of selected links increases with an increase of N , incurring the topology of snapshots becoming more diversified and dissimilar, so that α reduces with increasing N . As for β , since adjacent topology snapshots become more different as N increases, and snapshots whose dissimilarity exceeds φ cannot be simplified/merged, β reduces with an increase of N . As for $\chi(\Delta t)$, we can see from Fig. 12 that it is independent of N . This is because $S_{ED}(\Delta t)$ is only determined by T and Δt , hence incurring $\chi(\Delta t)$ invariant with N . In practice, although we

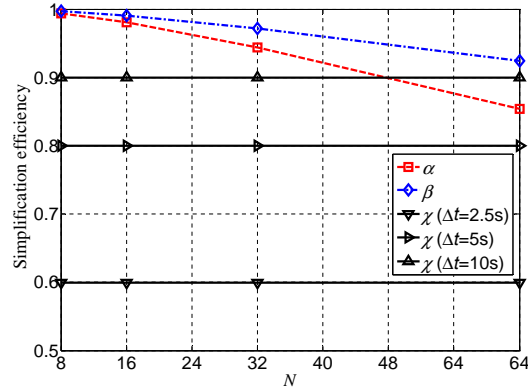


Fig. 12. Simplification efficiency vs. N under $\varphi = 3$.

can employ large Δt to get high $\chi(\Delta t)$, it should be noticed that since micro/nano satellite network topology doesn't vary with time uniformly, we will lose some topology information (*i.e.*, although network topology varies, only those change at moments $0, \Delta t, 2\Delta t, \dots, T$ are recorded in $S_{ED}(\Delta t)$), and moreover some redundant topologies may be maintained unnecessarily (*i.e.*, there are still duplicate snapshots in $S_{ED}(\Delta t)$). As a comparison, the proposed ICRTC can effectively avoid such deficiencies. Moreover, as Δt grows, more topology snapshots are simplified, hence yielding an increase of $\chi(\Delta t)$.

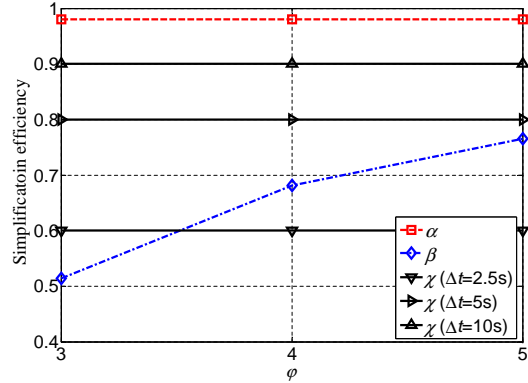


Fig. 13. Simplification efficiency vs. φ under $N = 16$.

Fig. 13 plots the variation of α , β and $\chi(\Delta t)$ with $\varphi \in \{3, 4, 5\}$ under $N = 16$. Monte-carlo simulation is adopted to obtain the average efficiency. As the figure shows, α remains constant as φ varies whereas β grows with an increase of φ . This is because φ only affects the execution of redundancy-increasing based simplification, hence α is independent of φ . As for β , since more snapshots are merged as φ grows, yielding an increase of the number of simplified snapshots, thus β increases as φ grows. As for $\chi(\Delta t)$, we can see from the figure that it remains constant as φ varies. The analysis can be found in the discussions about Fig. 12.

Fig. 14 compares the total number of selected links in snapshot sequences S_{DR} , S_{IC}

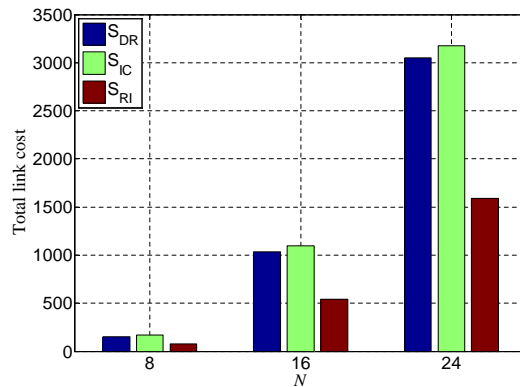


Fig. 14. Total link costs of different snapshot sequences vs. N .

and S_{RI} under different N s. The results are obtained via averaging 100 simulation samples. In each sample, the simulation time is taken 60 minutes. As the figure shows, the total number of links in snapshot sequences S_{DR} , S_{IC} and S_{RI} increase as N grows. Since S_{IC} is obtained by applying ICRTC in each snapshot in S_{DR} , redundant links are added to improve network's robustness, the number of links in S_{IC} slightly exceeds that in S_{DR} . As for the redundancy-increasing based simplification, although some redundant links are added, the total number of snapshots in S_{RI} is significantly reduced (which can be found in the simulation results in Fig. 10), yielding the total number of snapshots in S_{RI} decreases. That is, the proposed offline realization of ICRTC can effectively reduce the cost for topology control.

7. CONCLUDING REMARKS

In this paper, we propose an incremental-compensation based robust topology control (ICRTC) method and its low-cost offline realization for micro/nano satellite network. By establishing backup link(s) w.r.t. the fragile ones associated with high-failure-probability nodes, ICRTC can enhance the network's robustness with proper link redundancy cost. Moreover, by dividing the orbit period into snapshot sequence and simplifying it via combining the successive snapshots with the same topology and merging similar snapshots by adding a few redundant links, ICRTC can be implemented in an offline manner with reduced snapshots redundancy. Our simulation results have verified the effectiveness of and shown the benefits brought by ICRTC. Moreover, we have shown that the topology control overhead can be effectively reduced with the proposed offline realization.

APPENDICES: A. PROOF OF EQ. (6)

We first define function $F(l) = \Phi_{\{V_i^*, (\xi_l), V_j^*\}, \tau}$ for the ease of presentation where ξ_l denotes the link set constituting the l th path of node-pair $\{V_i^*, V_j^*\}$ while excluding the

two links associated with the end nodes V_i^* and V_j^* . Then, Eq. (6) can be simplified as:

$$\begin{aligned} \Phi_{\{V_i^*, V_j^*\}, \tau}^{[\Psi]} &= (-1)^0 \sum_{l=1}^{\Psi} F(l) + (-1)^1 \sum_{l=1}^{\Psi-1} \sum_{m=l+1}^{\Psi} F(l)F(m) \\ &\quad + (-1)^2 \sum_{l=1}^{\Psi-2} \sum_{m=l+1}^{\Psi-1} \sum_{q=l+2}^{\Psi} F(l)F(m)F(q) \\ &\quad + \cdots + (-1)^{\Psi-1} \prod_{l=1}^{\Psi} F(l). \end{aligned} \quad (8)$$

When $\Psi = 1$, we can have $\Phi_{\{V_i^*, V_j^*\}, \tau}^{[1]} = F(1)$, so that Eqs. (8) and (6) hold.

Next, we assume Eq. (8) holds under $\Psi = k$ and can get:

$$\begin{aligned} \Phi_{\{V_i^*, V_j^*\}, \tau}^{[k]} &= (-1)^0 \sum_{l=1}^k F(l) + (-1)^1 \sum_{l=1}^{k-1} \sum_{m=l+1}^k F(l)F(m) \\ &\quad + (-1)^2 \sum_{l=1}^{k-2} \sum_{m=l+1}^{k-1} \sum_{q=l+2}^k F(l)F(m)F(q) \\ &\quad + \cdots + (-1)^{k-1} \prod_{l=1}^k F(l) \end{aligned} \quad (9)$$

Then, given $\Psi = k+1$, we can have Eq. (10) according to $P(A \cup B) = P(A) + P(B) - P(A \cap B)$:

$$\Phi_{\{V_i^*, V_j^*\}, \tau}^{[k+1]} = \Phi_{\{V_i^*, V_j^*\}, \tau}^{[k]} + F(k+1) - \Phi_{\{V_i^*, V_j^*\}, \tau}^{[k]} F(k+1). \quad (10)$$

Substituting Eq. (9) into Eq. (10) and simplifying the expression, we have

$$\begin{aligned} \Phi_{\{V_i^*, V_j^*\}, \tau}^{[k+1]} &= (-1)^0 \sum_{l=1}^{k+1} F(l) \\ &\quad + [(-1)^1 \sum_{l=1}^{k-1} \sum_{m=l+1}^k F(l)F(m) + (-1)^1 F(k+1) \sum_{l=1}^k F(l)] \\ &\quad + [(-1)^2 \sum_{l=1}^{k-2} \sum_{m=l+1}^{k-1} \sum_{q=l+2}^k F(l)F(m)F(q) + (-1)^2 F(k+1) \sum_{l=1}^{k-1} \sum_{m=l+1}^k F(l)F(m)] \\ &\quad + \cdots + (-1)^k \prod_{l=1}^{k+1} F(l). \end{aligned} \quad (11)$$

We let $A = (-1)^1 \sum_{l=1}^{k-1} \sum_{m=l+1}^k F(l)F(m) + (-1)^1 F(k+1) \sum_{l=1}^k F(l)$ and can have:

$$\begin{aligned} A &= (-1)^1 \left\{ \sum_{l=1}^{k-1} F(l) \left[\sum_{m=l+1}^k F(m) + F(k+1) \right] + F(k+1) F(k) \right\} \\ &= (-1)^1 \left[\sum_{l=1}^{k-1} F(l) \sum_{m=l+1}^{k+1} F(m) + F(k+1) F(k) \right] \\ &= (-1)^1 \sum_{l=1}^k F(l) \sum_{m=l+1}^{k+1} F(m). \end{aligned} \quad (12)$$

Then, we let $B = (-1)^2 \sum_{l=1}^{k-2} \sum_{m=l+1}^{k-1} \sum_{q=l+2}^k F(l)F(m)F(q) + (-1)^2 F(k+1) \sum_{l=1}^{k-1} \sum_{m=l+1}^k F(l)F(m)$. Similarly to the derivation of Eq. (12), we can have:

$$B = (-1)^2 \sum_{l=1}^{k-1} F(l) \sum_{m=l+1}^k F(m) \sum_{q=l+2}^{k+1} F(q). \quad (13)$$

Therefore, Eq. (14) can be derived as:

$$\begin{aligned} \Phi_{\{V_i^*, V_j^*\}, \tau}^{[k+1]} &= (-1)^0 \sum_{l=1}^{k+1} F(l) + (-1)^1 \sum_{l=1}^k F(l) \sum_{m=l+1}^{k+1} F(m) \\ &\quad + (-1)^2 \sum_{l=1}^{k-1} F(l) \sum_{m=l+1}^k F(m) \sum_{q=l+2}^{k+1} F(q) \\ &\quad + \cdots + (-1)^k \prod_{l=1}^{k+1} F(l). \end{aligned} \quad (14)$$

We substitute $\Psi = k+1$ into Eq. (8) and can find that the result is the same as Eq. (14). Therefore, Eqs. (6) and (8) follow. ■

ACKNOWLEDGMENT

This work was supported in part by the Project of National Key Laboratory of Science and Technology on Space Microwave; NSF of Shaanxi Province under Grant 2021JM-143; Science and Technology Development Programme of Henan Province under Grant Number 212102210563; the Fundamental Research Funds for the Central Universities under Grant Number JB211502; the Project of Key Laboratory of Science and Technology on Communication Network under Grant Number 6142104200412; JSPS KAKENHI Grant Number JP20K14742; and the Project of Cyber Security Establishment with Inter University Cooperation.

REFERENCES

1. R. Zhang, F. Liu, and Y. Ding, "An energy optimization-based fast rerouting method for micro-nano satellite formation," in *Proceedings of IEEE 2nd International Conference on Electronics Technology*, 2019, pp. 131-136.
2. Y. Liu, L. Tian, J. Yang, *et al.*, "Communication system fast reconstruction strategy and efficiency simulation based on micro-nano satellites," in *Proceedings of the 8th International Conference on Instrumentation and Measurement, Computer, Communication and Control*, 2018, pp. 1156-1159.
3. K. Li, Q. Wang, Q. Zhang, *et al.*, "Vision autonomous relative navigation algorithm for distributed micro/nano satellite earth observation system based on motor Algebra," in *Proceedings of International Conference on Environmental Science and Information Application Technology*, 2009, pp. 470-473.
4. L. Yang and J. Sun, "Multi-service routing algorithm based on geo/leo satellite networks," in *Proceedings of International Conference on Network and Information Systems for Computers*, 2016, pp. 80-84.
5. L. Yongjun, Z. Shanghong, W. Jili, *et al.*, "Designing of a novel optical two-layered satellite network," in *Proceedings of International Conference on Computer Science and Software Engineering*, 2008, pp. 976-979.
6. L. Alexandru and P. Valentin, "Performance evaluation of topology control algorithms that can be integrated into a street lighting control sensor network," in *Proceedings of the 11th Roedunet International Conference*, 2013, pp. 1-4.
7. J. Pan, Y. Hou, C. Lin, *et al.*, "Topology control for wireless sensor networks," in *Proceedings of the 9th Annual International Conference on Mobile Computing and Networking*, 2003, pp. 286-299.
8. N. Li, J. C. Hou, and L. Sha, "Design and analysis of MST-based topology control algorithm," in *Proceedings of the 22nd Annual Joint Conference of the IEEE Computer and Communication Societies*, 2003, pp. 1702-1712.
9. H. Li and H. Qian, "Research on topology control in wireless ad hoc networks," in *Proceedings of International Conference on Internet Technology and Applications*, 2010, pp. 1-4.
10. M. Bahramgiri, M. Hajlaghayi, and V. S. Mirrokni, "Fault-tolerant and 3-dimensional distributed topology control algorithms in wireless multi-hop networks," in *Proceed-*

ings of the 11th International Conference on Computer Communications and Networks, 2002, pp. 392-397.

11. N. Li and J. Hou, "FLSS: A fault-tolerant topology control algorithm for wireless networks," in *Proceedings of the 10th Annual International Conference on Mobile Computing and Networking*, 2004, pp. 275-286.
12. Q. Chen, J. Zhang, and Z. Hu, "A topology control strategy with reliability assurance for satellite cluster networks in earth observation," *Sensors*, Vol. 17, 2017, pp. 445-463.
13. W. Zhang, G. Zhang, *et al.*, "A hierarchical autonomous system based space information network architecture and topology control," *Journal of Communications and Information Networks*, Vol. 1, 2017, pp. 77-89.
14. L. Kai, Z. Yubing, *et al.*, "A hybrid topology for distributed satellite clusters," *Journal Terahertz Science and Electronic Information Technology*, Vol. 17, 2019, pp. 1086-1090.
15. J. Wang, L. Li, and M. Zhou, "Topological dynamics characterization for LEO satellite networks," *Computer Networks*, Vol. 51, 2007, pp. 43-53.
16. A. Papa, T. de Cola, *et al.*, "Design and evaluation of reconfigurable SDN LEO constellations," *IEEE Transactions on Network and Service Management*, Vol. 17, 2020, pp. 1432-1445.
17. D. Bhattacharjee and A. Singla, "Network topology design at 27,000 km/hour," in *Proceedings of ACM International Conference on Emerging Networking Experiment and Technologies*, 2019, pp. 341-354.
18. Y. Zhao, X. Yi, and Z. Hou, "Topology-adapting routing strategy for global navigation satellite system," *International Journal Distributed Sensor Networks*, Vol. 13, 2017, pp. 1-13.
19. Q. Chen, J. Guo, *et al.*, "Topology virtualization and dynamics shielding method for LEO satellite networks," *IEEE Communications Letters*, Vol. 24, 2019, pp. 433-437.
20. Z. Tang, Z. Feng, *et al.*, "Improving the snapshot routing performance through reassigning the inter-satellite links," in *Proceedings of IEEE International Conference on Computer Communications*, 2015, pp. 97-98.
21. X. Jia, T. Lv, *et al.*, "Collaborative data downloading by using inter-satellite links in LEO satellite networks," *IEEE Transactions on Wireless Communications*, Vol. 16, 2017, pp. 1523-1532.
22. W. Zhang, G. Zhang, *et al.*, "A hierarchical autonomous system based topology control algorithm in space information network," *KSI Transactions on Internet and Information Systems*, Vol. 9, 2015, pp. 3572-3593.
23. M. Huang, S. Chen, *et al.*, "Topology control for time-evolving and predictable delay-tolerant networks," *IEEE Transactions on Computers*, Vol. 62, 2013, pp. 2308-2321.
24. E. Lee, "A micro HTS renewable energy/attitude control system for micro/nano satellites," *IEEE Transactions on Applied Superconductivity*, Vol. 13, 2003, pp. 2263-2266.
25. N. Ye, Z. Zhu, J. Liu, *et al.*, "Distributed cluster-based fault-tolerant topology control for space information networks," in *Proceedings of IEEE International Conference on Cyber-Enabled Distributed Computing and Knowledge Discovery*, 2010, pp. 210-217.

26. A. S. Korad and K. N. Hedman, "Robust corrective topology control for system reliability," *IEEE Transactions on Power Systems*, Vol. 28, 2013, pp. 4042-4051.
27. L. K. Herman, "The history, definition and peculiarities of the Earth Centered Inertial (ECI) coordinate frame and the scales that measure time," in *Proceedings of IEEE Aerospace Applications Conference*, 1995, pp. 233-263.
28. Z. Li, Y. Hu, J.-L. Li, and L.-Y. Xiao, "Tracing compensation robust topology control method and system, medium, equipment and terminal," Patent No. 202011233838.7, Xi'an Institute of Space Radio Technology, Xidian University, 2020.
29. T. H. Cormen, C. E. Leiserson, *et al.*, *Introduction to Algorithms*, 3rd ed., The MIT Press, Cambridge, 2009.



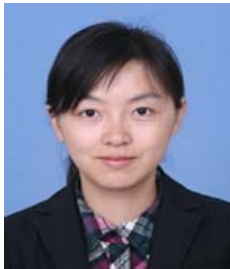
Zhao Li received the BS degree in Telecommunications Engineering, the MS and Ph.D. degrees in Communication and Information Systems from Xidian University, Xi'an, China, in 2003, 2006, and 2010, respectively. He is currently an Associate Professor in the School of Cyber Engineering, Xidian University. He worked as a Visiting Scholar and then Research Scientist in the Real-Time Computing Laboratory in the Department of Electrical Engineering and Computer Science, The University of Michigan, during 2013-2015. He has published over 40 technical papers at premium international journals and conferences such as IEEE TWC, IEEE IoT Journal, IEEE INFOCOM, IEEE TVT, Computer Communications, and so on. His research interests include wireless communication, 5G communication systems, resource allocation, interference management, IoT and physical layer security.



Yuyu Hu is currently a Master student in the School of Cyber Engineering at Xidian University. Her research interests include wireless communication, topology control algorithm design, and network performance evaluation.



Zhendong Hu is currently a Master student in the School of Cyber Engineering at Xidian University. His research interests include wireless communication, topology control algorithm design, and network simulation.



Jingling Li received the BS degree in Communication Engineering and the MS degree in Communication and Information Systems from Xidian University, Xi'an, China, in 2006 and 2009, respectively. She is currently a Senior Engineer in National Key Laboratory of Science and Technology on Space Microwave, CAST Xi'an. Her research interests include satellite communication, satellite processing and spatial information network.



Shitong Zhu is currently a Master student in the School of Cyber Engineering at Xidian University. His research interests include wireless communication and network simulation.



Yang Xu received the B.E. degree from the School of Telecommunications Engineering and the Ph.D. degree from the Department of Communication and Information Systems, Xidian University, Xi'an, China, in 2006 and 2014, respectively, where she is currently a Lecturer with the School of Economics and Management, The State Key Laboratory of Integrated Services Network. She has published about 30 papers at premium international journals, including IEEE IoT Journal, IEEE TWC, IEEE TVT, and Computer Networks. She has published in conferences including IEEE ICC and IEEE WCNC. Her current research interests include physical layer security, block-chain, routing protocol design and network performance evaluation.